Letter

Orbital mixing at the onset of high-temperature superconductivity in $FeSe_{1-x}Te_x/CaF_2$

K. Nakayama,[1,2] R. Tsubono,[1] G. N. Phan,[1,*] F. Nabeshima,[3] N. Shikama,[3] T. Ishikawa,[3] Y. Sakishita,[3] S. Ideta,[4,5] K. Tanaka,[4,5] A. Maeda,[3] T. Takahashi,[1,6,7] and T. Sato[1,6,7]

[1]*Department of Physics, Tohoku University, Sendai 980-8578, Japan*

[2]*Precursory Research for Embryonic Science and Technology, Japan Science and Technology Agency, Tokyo 102-0076, Japan*

[3]*Department of Basic Science, University of Tokyo, 3-8-1 Komaba, Meguro, Tokyo 153-8902, Japan*

[4]*UVSOR Synchrotron Facility, Institute for Molecular Science, Okazaki 444-8585, Japan*

[5]*School of Physical Sciences, The Graduate University for Advanced Studies (SOKENDAI), Okazaki 444-8585, Japan*

[6]*Center for Spintronics Research Network, Tohoku University, Sendai 980-8577, Japan*

[7]*WPI Research Center, Advanced Institute for Materials Research, Tohoku University, Sendai 980-8577, Japan*

(Received 15 September 2020; revised 5 January 2021; accepted 7 January 2021; published 20 January 2021)

We perform systematic high-resolution angle-resolved photoemission spectroscopy of iron-chalcogenide superconductor $FeSe_{1-x}Te_x$ films on CaF_2 which exhibit a unique paramagnetic nematicity at $x = 0$ (pristine FeSe) and a gigantic T_c enhancement at the critical Te concentration (x_c) of $x \sim 0.2$. Upon increasing the Te concentration from $x = 0$, the electronlike Fermi-surface shape at the Brillouin-zone corner shows a clear change associated with a remarkable energy shift of the $d_{xz/yz}$ orbital, indicative of the suppression of nematicity near x_c. Evolution of band structure at the Brillouin-zone center is characterized by a drastic upward shift of the d_{xy} band with increasing x, leading to an orbital switching from $d_{xz/yz}$ to $d_{xz/yz} + d_{xy}$ accompanied by a mass enhancement. These results demonstrate that the pristine and high-T_c $FeSe_{1-x}Te_x$ have distinctly different electronic structures. The present study lays the foundation for understanding the origin of high-T_c superconductivity and the interplay with electronic nematicity.

DOI: 10.1103/PhysRevResearch.3.L012007

Iron-based high-temperature T_c superconductors are a multiorbital system, in which all five Fe $3d$ orbitals are involved in the low-energy electronic structure. As an emergent phenomenon associated with the multiorbital nature, the electronic nematicity, defined as a spontaneous breaking of rotational symmetry [1–8], is at the forefront of research in condensed-matter physics. The nematic state is widely observed near the superconducting state in iron-based superconductors, so particular interest is focused on the interplay between nematicity and superconductivity. However, the nematicity is strongly coupled to the collinear-type antiferromagnetic order accompanied by a tetragonal-to-orthorhombic structural transition [9], which makes it difficult to isolate the influence of nematicity from antiferromagnetism.

Among iron-based superconductors, FeSe [10,11] is a unique system showing nematicity without antiferromagnetic order. Because of this unique property, recent studies on FeSe have revealed several important insights into nematicity and the impact on superconductivity, such as a large energy shift of the d_{xz} and d_{yz} bands due to the lifting of orbital degeneracy around the structural transition temperature $T_s \sim 90$ K [12–17] and a signature of orbital-selective pairing below T_c [18–21]. FeSe also has a great advantage in tunability of superconductivity through chemical substitution [22–24], high-pressure application [25,26], and/or carrier doping [27–29]. Therefore, one can investigate the interplay between nematicity and superconductivity by precisely tracing the evolution of the electronic structure responsible for nematicity and superconductivity while controlling some physical parameters. In this respect, isovalent-substituted $FeSe_{1-x}Te_x$ films grown on CaF_2 substrate ($FeSe_{1-x}Te_x/CaF_2$) offer an excellent platform because the nematicity without antiferromagnetic order is realized in $FeSe/CaF_2$ ($x = 0$) as in bulk FeSe [30,31] and the highest T_c of 23 K among non-carrier-doped FeSe-based compounds has been reported at the critical Te concentration x_c of ~0.2 at ambient pressure [23,24,32] [Fig. 1(a)] (note that bulk $FeSe_{1-x}Te_x$ crystals of $0.1 < x < 0.4$ were unavailable due to the phase separation [22]). It is thus desirable to determine experimentally the electronic structure of $FeSe_{1-x}Te_x/CaF_2$ as a function of x.

Angle-resolved photoemission spectroscopy (ARPES) is the best suited technique to probe the momentum-resolved electronic structure. However, there is no systematic ARPES report on $FeSe_{1-x}Te_x/CaF_2$ with a series of different x values, mainly due to the difficulties in fabricating $FeSe_{1-x}Te_x/CaF_2$ and in preparing a clean surface necessary for ARPES measurements. In this Letter, by overcoming these difficulties, we report a systematic ARPES study on the evolution of

*Present address: Beijing National Laboratory for Condensed Matter Physics and Institute of Physics, Chinese Academy of Sciences, Beijing 100080, China.

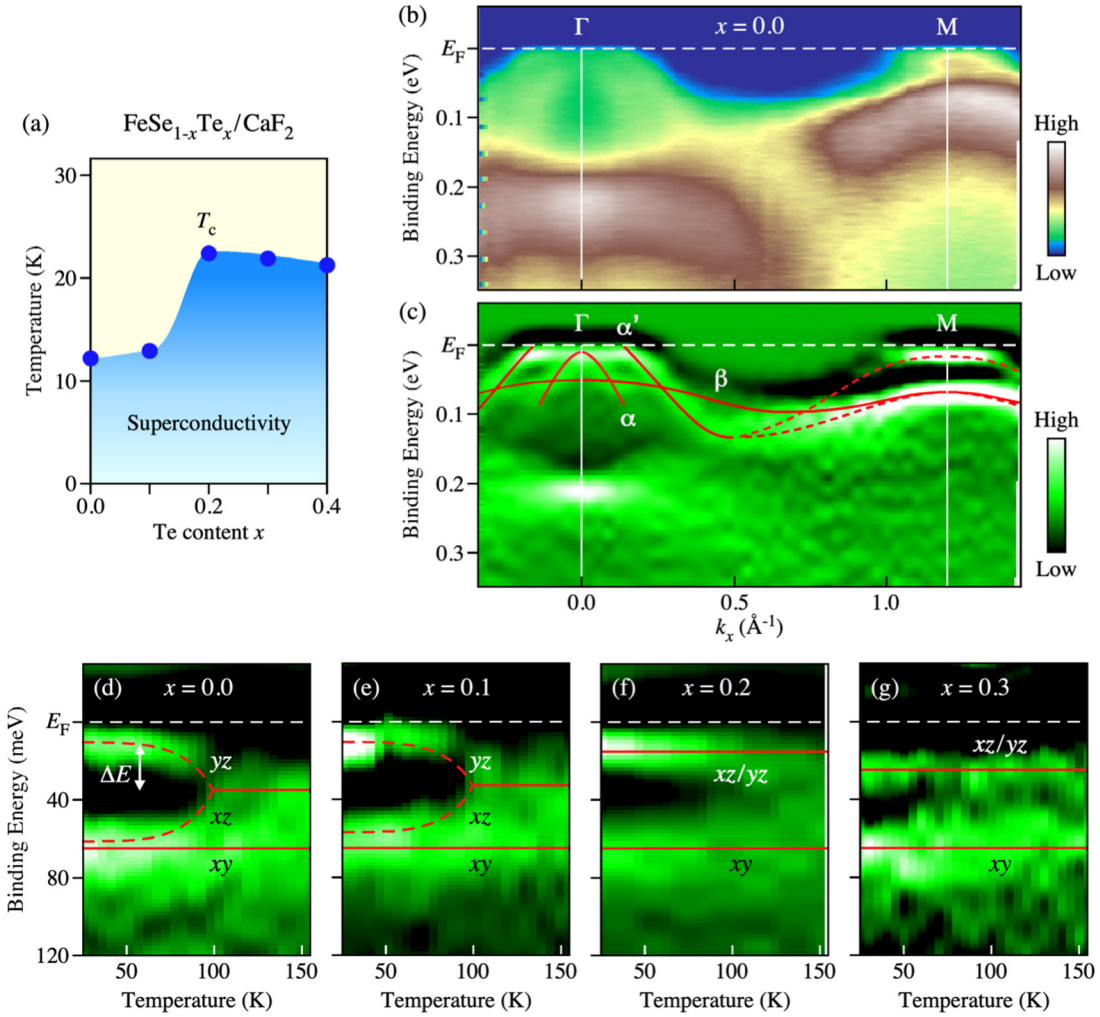

FIG. 1. (a) Phase diagram of $FeSe_{1-x}Te_x/CaF_2$ as a function of Te concentration x [23]. Also shown are plots of (b) the APRES intensity and (c) the corresponding second-derivative intensity, measured along the Γ-M line at $T = 30$ K for $FeSe/CaF_2$ ($x = 0$) with linearly polarized 21.2-eV photons. The temperature dependence of the second-derivative ARPES intensity at the M point is shown for (d) $x = 0$, (e) $x = 0.1$, (f) $x = 0.2$, and (g) $x = 0.3$. The red curves in (c)–(g) are a guide for the eyes to trace the band dispersions.

the electronic structure in $FeSe_{1-x}Te_x/CaF_2$ over a wide x range ($0 \leqslant x \leqslant 0.4$). We reveal the suppression of nematicity on approaching x_c, indicative of the anticorrelation between nematicity and superconductivity. We also find evidence for the electronic reconstruction near the Fermi level E_F characterized by switching of the Fe 3d orbital character. We discuss implications of our observation in relation to the origin of T_c enhancement and the suppression of nematicity.

High-quality $FeSe_{1-x}Te_x$ films ($x = 0$–0.4) with a thickness of approximately 400 unit cells were grown on CaF_2 by pulsed-laser-deposition method. These films are compressively strained, so $FeSe/CaF_2$ ($x = 0$) shows a higher T_c (12 K) than the bulk counterpart (∼9 K) [33]. Details of film growth and their characterization are described elsewhere [23,32–34]. The ARPES measurements were performed with MBS-A1 and Scienta-Omicron-SES2002 electron analyzers at BL7U in UVSOR and Tohoku University, respectively. We used 21.2-eV photons. The energy and angular resolutions were set to be 12–30 meV and 0.2°–0.3°, respectively. A clean surface for ARPES measurements was obtained by cleaving the films *in situ* in an ultrahigh vacuum. We note that $FeSe_{1-x}Te_x/CaF_2$ is often cleaved at the interface between $FeSe_{1-x}Te_x$ and CaF_2 and the resultant exposure of the CaF_2 surface prevents us from obtaining the ARPES data for the $FeSe_{1-x}Te_x$ layer. Nevertheless, we have cleaved more than 70 samples and obtained a clean $FeSe_{1-x}Te_x$ surface.

Figures 1(b) and 1(c) show plots of the ARPES intensity and corresponding second-derivative intensity, respectively, along the Γ-M line of the Brillouin zone at $T = 30$ K for pristine $FeSe/CaF_2$ ($x = 0$ and $T_c = 12$ K). The near-E_F band structure around the Γ point consists of two highly dispersive bands α and α' and a relatively flat band β [see red curves in Fig. 1(c)]. According to previous studies, the α and α' bands are ascribed to the Fe $3d_{xz}/d_{yz}$ orbitals and the β band is ascribed to the Fe $3d_{xy}$ orbital [12–17,30]. Around the M point, there are two holelike bands topped at binding energies E_B of ∼20 and ∼70 meV, which are attributed to the d_{yz}- and d_{xz}-derived bands originating from a splitting of the α' band due to the lifting of orbital degeneracy [see red dashed curves in Fig. 1(c)] [12–17] because $FeSe/CaF_2$ is in the nematic state at 30 K [30,31]. In fact, a temperature-dependent study at the M point reveals a large downward shift

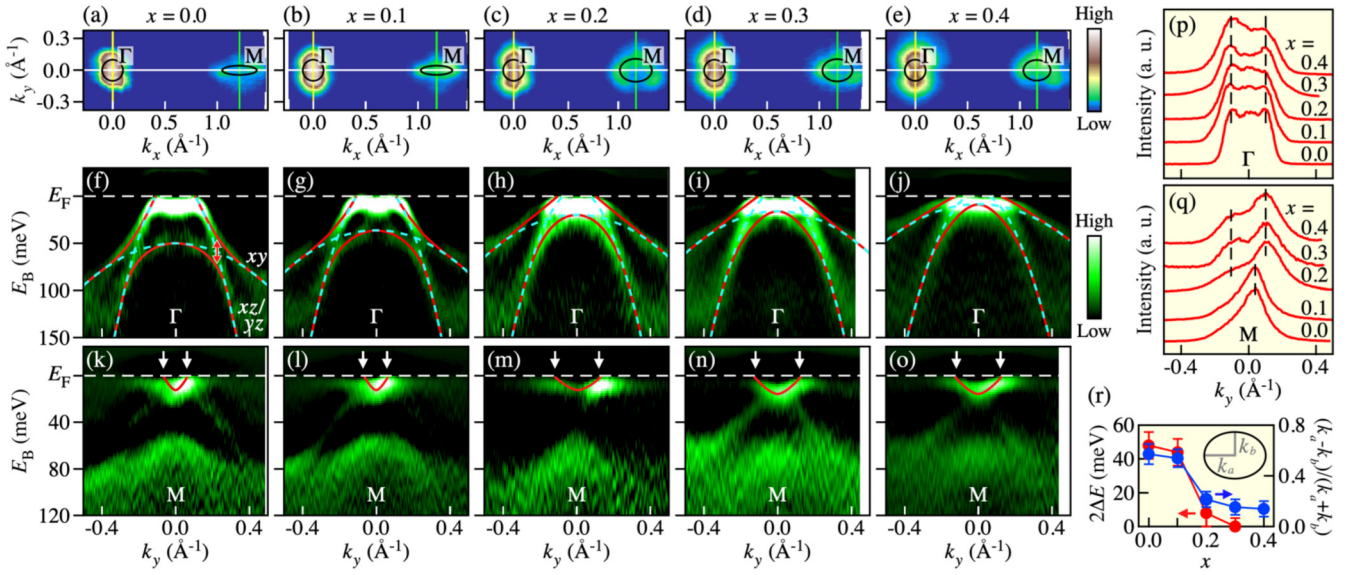

FIG. 2. Te-concentration dependence of the ARPES-intensity map at E_F as a function of the two-dimensional wave vector for $FeSe_{1-x}Te_x/CaF_2$, with (a) $x = 0.0$, (b) $x = 0.1$, (c) $x = 0.2$, (d) $x = 0.3$, and (e) $x = 0.4$, at $T = 30$ K. Black curves are the schematic of FSs. Also shown is the near-E_F second-derivative ARPES intensity obtained at $T = 30$ K along yellow and green lines, around the (f)–(j) Γ and (k)–(o) M points, in (a)–(e), respectively. Cyan and red curves are a guide for the eyes to trace the band dispersions before and after hybridization, respectively. The band dispersions before the hybridization were estimated by extrapolating the dispersions determined in the $(E, \mathbf{k})$ region away from the intersection point. (p) and (q) Comparison of momentum distribution curves at E_F extracted from (f)–(j) and (k)–(o), respectively. Dashed lines are a guide for the eyes to trace the peak position. (r) Te-concentration dependence of an anisotropy of the electronlike FS $(k_a - k_b)/(k_a + k_b)$ (blue circles), compared with the nematic energy scale $2\Delta E$ (red circles) approximated as twice the energy difference of the d_{yz} band between $T = 30$ and 110 K.

($\Delta E = 24$ meV) of the d_{yz} band with increasing temperature [Fig. 1(d)], consistent with the occurrence of nematicity (note that an upward shift expected for the d_{xz} counterpart is not clearly resolved due to an energy overlap with the β band at higher E_B). To clarify the evolution of nematicity with Te substitution, we performed temperature-dependent studies at the M point for $x = 0.1$–0.3. A side-by-side comparison [Figs. 1(d)–1(g)] reveals that the d_{yz} band shows a large energy shift with increasing temperature at $x = 0.1$, similarly to the observation at $x = 0$, whereas the d_{yz} band is almost stationary with temperature at $x = 0.2$ and 0.3. This strongly suggests that the nematic state is destroyed at $x \sim x_c$. The suppression of nematicity while approaching $x = x_c$ demonstrates the anticorrelation between nematicity and T_c in $FeSe_{1-x}Te_x/CaF_2$.

To investigate how the band structure changes across x_c, we performed systematic measurements of the Fermi surface (FS) [Figs. 2(a)–2(e)] and the band dispersion [Figs. 2(f)–2(o)] for five different compositions. One can recognize that the FS shape around the M point is elongated along the k_x axis for $x \leqslant 0.1$, whereas it is more rounded for $x \geqslant 0.2$ [Figs. 2(a)–2(e)]. This change is fairly drastic, as evidenced by a jump in the Fermi wave vector k_F of the electron-band dispersion between $x = 0.1$ and 0.2 [see white arrows in Figs. 2(k)–2(o), the peak position of the momentum distribution curves at E_F in Fig. 2(q), and Fig. S1 in the Supplemental Material [35]]. To evaluate the FS anisotropy quantitatively, we assumed an elliptical shape for the electronlike FS and defined k_a and k_b as the k_F value along the major and minor axes, respectively [see the inset to Fig. 2(r)], to calculate a value of $(k_a - k_b)/(k_a + k_b)$ that gives a large (small) value when the FS is elongated (circular). The strong variation obtained at $x \sim 0.2$ [see red circles in Fig. 2(r)] confirms that the electronlike FS has a different shape between $x < x_c$ and $x \geqslant x_c$. Further, the x dependence of the FS anisotropy follows that of the estimated nematic energy scale $2\Delta E$, which corresponds to twice the d_{yz}-band energy shift in Figs. 1(d)–1(g) [blue circles in Fig. 2(r)], indicating that the FS anisotropy is linked to the presence/absence of nematicity, namely, the elongated shape of FS is triggered by the upward shift of the d_{yz} orbital [12–17].

To clarify the effect of Te substitution in more detail, we turn our attention to the Brillouin-zone center. It has been reported that, although the $d_{xz/yz}$-orbital degeneracy is lifted around the Γ point by nematicity as in the case of the M point, the energy difference between the d_{xz} and d_{yz} bands and the resultant change in the FS shape are relatively small [14,16,17]. Therefore, there is no discernible change in the holelike-FS shape within the present experimental accuracy [Figs. 2(a)– 2(e) and 2(p)]. Instead, a remarkable x dependence beyond the effect of nematicity manifests itself in the band dispersion [Figs. 2(f)–2(j)]. At $x = 0$, there are a highly dispersive $d_{xz/yz}$-band crossing E_F and a relatively flat d_{xy} band with the top of the dispersion at $E_B \sim 50$ meV (cyan dashed curves), which correspond to the α' and β bands, respectively, in Fig. 1(c) [note that the intensity of the inner $d_{xz/yz}$ band (α band) is suppressed due to the matrix-element effect]. These bands intersect with each other to open a hybridization gap of ∼25 meV caused by the spin-orbit coupling (SOC) [36] (the band dispersion after the hybridization is shown by red curves and the SOC-induced gap is highlighted by a red arrow). Intriguingly, the top of the d_{xy} band gradually shifts upward with increasing x and nearly touches E_F at $x = 0.4$

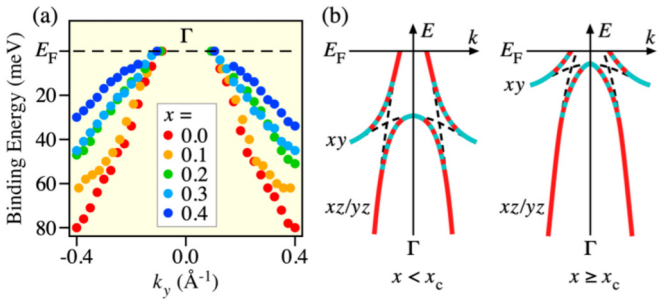

FIG. 3. (a) Comparison of the experimental near-E_F band dispersions extracted by tracing the peak position of ARPES spectra. (b) Schematics of the band structure around the Γ point for $x < x_c$ (left) and $x \geqslant x_c$ (right).

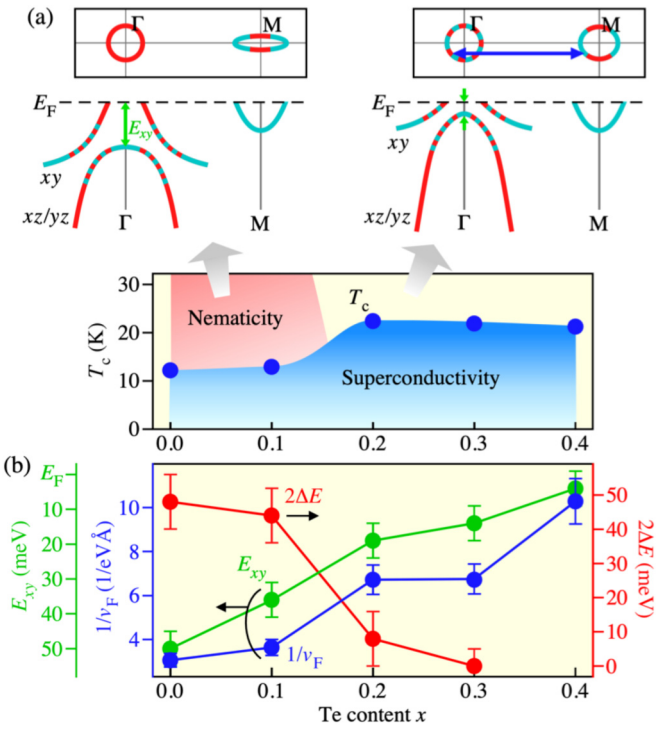

FIG. 4. (a) Schematic FSs and band dispersions at $T = 30$ K for $x < x_c$ (left) and $x \geqslant x_c$ (right), together with the phase diagram of $FeSe_{1-x}Te_x/CaF_2$. (b) Comparison of the x dependence of the nematic energy scale $2\Delta E$ [red circles; same as the data in Fig. 2(r)], energy position of the d_{xy}-derived hole band at Γ, E_{xy} (green circles), and an inverse of v_F for the hole pocket (blue circles).

(see also Fig. S2 in the Supplemental Material [35]). Due to such close proximity of the d_{xy} band to E_F, the electronic states at E_F are strongly modified for $x \geqslant 0.2$. Specifically, the hybridization of the $d_{xz/yz}$ band with the relatively flat d_{xy} band causes flattening of the band dispersion near E_F [Figs. 2(h)–2(j)], resulting in a decrease of Fermi velocity v_F for $x \geqslant 0.2$, as corroborated by a direct comparison of the near-E_F band dispersions in Fig. 3(a). On the other hand, the electronic states at E_F are intact for $x \leqslant 0.1$ because the d_{xy} band is well below E_F [Figs. 2(f) and 2(g)]. The quantitative analysis of experimental band dispersion in Fig. 3(a) shows that the v_F value for $x \geqslant 0.2$ is less than half that for $x \leqslant 0.1$, leading to an increase of the density of states (DOS) at E_F.

Another important outcome of the upward d_{xy}-band shift is the participation of the d_{xy} orbital with the holelike FS at $x \geqslant 0.2$. Although the top of the bare d_{xy} band before the hybridization does not reach E_F, this is enabled by the band hybridization. As schematically shown in Fig. 3(b), the band hybridization is expected to mix the $d_{xz/yz}$ and d_{xy} orbitals in the $(E, \mathbf{k})$ region where the energy bands show a hybridization-induced shift. Thus, the observed clear change in the band dispersion at E_F (i.e., change in the v_F value) for $x \geqslant 0.2$ strongly suggests the finite d_{xy}-orbital component at E_F (right panel). On the other hand, a negligible contribution from the d_{xy} orbital is expected at E_F for $x \leqslant 0.1$ because the influence of band hybridization does not reach E_F (left panel) [see also Figs. 2(f) and 2(g)]. Such consideration led us to conclude that the holelike FS consists of mixed $d_{xz/yz} + d_{xy}$ orbitals for $x \geqslant 0.2$, whereas it consists purely of the $d_{xz/yz}$ orbital for $x \leqslant 0.1$. We note that the upward energy shift of the d_{xy} band could be satisfactorily explained in terms of an increase of chalcogen height from the Fe plane [37], which is naturally expected from the larger ionic radius of Te than that of Se [22].

Now we discuss implications of the present ARPES results in relation to the gigantic T_c enhancement. Our main findings are the suppression of nematicity near x_c and the energy shift of the d_{xy} band. The former demonstrates that the high-T_c superconductivity anticorrelates with the nematicity in $FeSe_{1-x}Te_x$, as inferred from the anticorrelation between the superconductivity and the structural transition [32]. Such an anticorrelation implies that the two states are competing with each other or nematic/orbital fluctuations which potentially arise near the end point of the nematic phase may play a role in enhancing T_c [38–40]. Also, the latter finding, the d_{xy}-band shift, may be responsible for the T_c enhancement in two ways. First, as illustrated in the upper panel of Fig. 4(a) and also plotted by green circles in Fig. 4(b), the energy position of the d_{xy}-band top at the Γ point with respect to E_F [E_{xy}, indicated by the green arrow in Fig. 4(a)] gradually decreases upon Te substitution, likely due to a gradual change in the anion height, as expected from the smooth evolution of lattice constants over a whole x range [23] and, for $x \geqslant x_c$, the d_{xy} band is close enough to E_F to decrease v_F through the hybridization with the $d_{xz/yz}$ band, leading to an increase in the DOS at E_F around the Γ point. A simple estimation by assuming a linear scaling between the DOS and $1/v_F$ indicates that the large enhancement of DOS coincides with the appearance of high-T_c superconductivity at $x = x_c$ [see blue circles in Fig. 4(b)]. Therefore, the increase in the DOS (more than twice compared to that for $x < x_c$) due to the decrease of E_{xy} may contribute to the T_c enhancement at x_c. We note that the increase of $1/v_F$ by a factor of ∼2 is small compared to the large difference in the mass between the bare $d_{xz/yz}$ and d_{xy} bands because E_F is located in the vicinity of their crossing point where the band velocity rather gradually changes. Second, small E_{xy} also results in a transformation of the orbital character of the holelike FS from pure $d_{xz/yz}$ to mixed $d_{xz/yz} + d_{xy}$ near x_c [see the schematics in Fig. 4(a)]. The appearance of the d_{xy} orbital on the holelike FS promotes the intra-d_{xy}-orbital scattering between the hole and electron

pockets for $x \geqslant x_c$ [indicated by a blue arrow in the upper right panel of Fig. 4(a)] and enhances spin fluctuations in the d_{xy} channel. Such enhanced spin fluctuations in the d_{xy} channel, either alone [37] or in cooperation with orbital fluctuations [38,39], have been proposed to increase T_c. Therefore, our observations are compatible with the several routes to the T_c enhancement. Nevertheless, since T_c is usually determined by various parameters including effective interactions that are not solely controlled by the low-energy electronic structure, further experimental studies are desired to clarify the dominant source of high-T_c superconductivity, e.g., by determining the momentum/orbital dependence of the superconducting-gap size.

Next we discuss the possibility that the strength of nematicity is related to E_{xy}. The decrease of E_{xy} causes not only the appearance of the d_{xy}-orbital state on the holelike FS, but also the reduction of the $d_{xz/yz}$-orbital state for $x \geqslant x_c$, which in turn suppresses the spin fluctuation in the $d_{xz/yz}$ channel. According to the self-consistent vertex correlation theory, the reduction of spin fluctuation in the $d_{xz/yz}$ channel suppresses the nematicity because the orbital susceptibility is reduced through the orbital-spin interplay [39]. Although this theory is constructed to explain the phase diagram of FeSe under high pressure, the conceptually same situation is realized in $FeSe_{1-x}Te_x/CaF_2$. Therefore, besides the large electronic and orbital reconstructions around the zone corner, the decrease of E_{xy} around the zone center may play an additional role in suppressing the nematicity in $FeSe_{1-x}Te_x/CaF_2$.

Finally, we comment on the role of SOC. As described above, when the SOC is absent, the d_{xy} hole band seems to be located below E_F for all samples measured in this study. In other words, the appearance of the d_{xy} state and the mass enhancement at E_F are realized not solely by the upward shift of d_{xy} band but also by the assistance of SOC. Therefore, SOC may indirectly contribute to the increase in T_c and the suppression of nematicity at $x \geqslant x_c$.

In conclusion, the present systematic high-resolution ARPES study has revealed a drastic energy shift of the d_{xy} band which results in the participation of the d_{xy} orbital in the formation of a holelike FS at $x \geqslant x_c$. In addition, the suppression of nematicity has been found near x_c, indicating the anticorrelation between the high-T_c superconductivity and the nematicity. These findings established distinct electronic structures with different orbital occupations between the pristine and high-T_c $FeSe_{1-x}Te_x/CaF_2$. The present results provide important insights into the interplay among high-T_c superconductivity, nematicity, and orbital degrees of freedom.

We thank Y. Kubota and K. Owada for their assistance with the ARPES measurements. We also thank UVSOR for access to beamlines BL7U and BL5U (Proposals No. 30-554, No. 19-568, and No. 19-857). This work was supported by JST-PRESTO (Grant No. JPMJPR18L7), JST-CREST (Grant No. JPMJCR18T1), and Grant-in-Aid for Scientific Research (JSPS KAKENHI Grants No. JP17H04847, No. JP17H01139, No. JP18H01160, No. JP19K14651, and No. JP20H01847).

[1] T.-M. Chuang, M. P. Allan, J. Lee, Y. Xie, N. Ni, S. L. Bud'ko, G. S. Boebinger, P. C. Canfield, and J. C. Davis, Science **327**, 181 (2010).

[2] J.-H. Chu, J. Analytis, K. De Greve, P. McMahon, Z. Islam, Y. Yamamoto, and I. Fisher, Science **329**, 824 (2010).

[3] M. A. Tanatar, E. C. Blomberg, A. Kreyssig, M. G. Kim, N. Ni, A. Thaler, S. L. Bud'ko, P. C. Canfield, A. I. Goldman, I. I. Mazin, and R. Prozorov, Phys. Rev. B **81**, 184508 (2010).

[4] A. Dusza, A. Lucarelli, F. Pfuner, J. H. Chu, I. R. Fisher, and L. Degiorgi, Europhys. Lett. **93**, 37002 (2011).

[5] M. Yi, D. Lu, J.-H. Chu, J. G. Analytis, A. P. Sorini, A. F. Kemper, B. Moritz, S.-K. Mo, R. G. Moore, M. Hashimoto, W.-S. Lee, Z. Hussain, T. P. Devereaux, I. R. Fisher, and Z.-X. Shen, Proc. Natl. Acad. Sci. U.S.A. **108**, 6878 (2011).

[6] S. Kasahara, H. J. Shi, K. Hashimoto, S. Tonegawa, Y. Mizukami, T. Shibauchi, K. Sugimoto, T. Fukuda, T. Terashima, Andriy H. Nevidomskyy, and Y. Matsuda, Nature (London) **486**, 382 (2012).

[7] J.-H. Chu, H.-H. Kuo, J. G. Analytis, and I. R. Fisher, Science **337**, 710 (2012).

[8] R. M. Fernandes, A. V. Chubukov, and J. Schmalian, Nat. Phys. **10**, 97 (2014).

[9] P. Dai, Rev. Mod. Phys. **87**, 855 (2015).

[10] F.-C. Hsu, J.-Y. Luo, K.-W. Yeh, T.-K. Chen, T.-W. Huang, Y.-C. Lee, Y.-L. Huang, Y.-Y. Chu, D.-C. Yan, and M.-K. Wu, Proc. Natl. Acad. Sci. U.S.A. **105**, 14262 (2008).

[11] T. M. McQueen, A. J. Williams, P. W. Stephens, J. Tao, Y. Zhu, V. Ksenofontov, F. Casper, C. Felser, and R. J. Cava, Phys. Rev. Lett. **103**, 057002 (2009).

[12] K. Nakayama, Y. Miyata, G. N. Phan, T. Sato, Y. Tanabe, T. Urata, K. Tanigaki, and T. Takahashi, Phys. Rev. Lett. **113**, 237001 (2014).

[13] T. Shimojima, Y. Suzuki, T. Sonobe, A. Nakamura, M. Sakano, J. Omachi, K. Yoshioka, M. Kuwata-Gonokami, K. Ono, H. Kumigashira, A. E. Böhmer, F. Hardy, T. Wolf, C. Meingast, H. v. Löhneysen, H. Ikeda, and K. Ishizaka, Phys. Rev. B **90**, 121111(R) (2014).

[14] Y. Suzuki, T. Shimojima, T. Sonobe, A. Nakamura, M. Sakano, H. Tsuji, J. Omachi, K. Yoshioka, M. Kuwata-Gonokami, T. Watashige, R. Kobayashi, S. Kasahara, T. Shibauchi, Y. Matsuda, Y. Yamakawa, H. Kontani, and K. Ishizaka, Phys. Rev. B **92**, 205117 (2015).

[15] P. Zhang, T. Qian, P. Richard, X. P. Wang, H. Miao, B. Q. Lv, B. B. Fu, T. Wolf, C. Meingast, X. X. Wu, Z. Q. Wang, J. P. Hu, and H. Ding, Phys. Rev. B **91**, 214503 (2015).

[16] M. D. Watson, T. K. Kim, A. A. Haghighirad, N. R. Davies, A. McCollam, A. Narayanan, S. F. Blake, Y. L. Chen, S. Ghannadzadeh, A. J. Schofield, M. Hoesch, C. Meingast, T. Wolf, and A. I. Coldea, Phys. Rev. B **91**, 155106 (2015).

[17] M. Yi, H. Pfau, Y. Zhang, Y. He, H. Wu, T. Chen, Z. R. Ye, M. Hashimoto, R. Yu, Q. Si, D.-H. Lee, P. Dai, Z.-X. Shen, D. H. Lu, and R. J. Birgeneau, Phys. Rev. X **9**, 041049 (2019).

[18] P. O. Sprau, A. Kostin, A. Kreisel, A. E. Böhmer, V. Taufour, P. C. Canfield, S. Mukherjee, P. J. Hirschfeld, B. M. Andersen, and J. C. S. Davis, Science **357**, 75 (2017).

[19] T. Hashimoto, Y. Ota, H. Q. Yamamoto, Y. Suzuki, T. Shimojima, S. Watanabe, C. Chen, S. Kasahara, Y. Matsuda,

T. Shibauchi, K. Okazaki, and S. Shin, Nat. Commun. **9**, 282 (2018).

[20] L. C. Rhodes, M. D. Watson, A. A. Haghighirad, D. V. Evtushinsky, M. Eschrig, and T. K. Kim, Phys. Rev. B **98**, 180503(R) (2018).

[21] D. Liu, C. Li, J. Huang, B. Lei, L. Wang, X. Wu, B. Shen, Q. Gao, Y. Zhang, X. Liu, Y. Hu, Y. Xu, A. Liang, J. Liu, P. Ai, L. Zhao, S. He, L. Yu, G. Liu, Y. Mao *et al.*, Phys. Rev. X **8**, 031033 (2018).

[22] Y. Mizuguchi and Y. Takano, J. Phys. Soc. Jpn. **79**, 102001 (2010).

[23] Y. Imai, Y. Sawada, F. Nabeshima, and A. Maeda, Proc. Natl. Acad. Sci. U.S.A. **112**, 1937 (2015).

[24] J. Zhuang, W. K. Yeoh, X. Cui, X. Xu, Y. Du, Z. Shi, S. P. Ringer, X. Wang, and S. X. Dou, Sci. Rep. **4**, 7273 (2014).

[25] S. Medvedev, T. M. McQueen, I. A. Troyan, T. Palasyuk, M. I. Eremets, R. J. Cava, S. Naghavi, F. Casper, V. Ksenofontov, G. Wortmann, and C. Felser, Nat. Mater. **8**, 630 (2009).

[26] K. Matsuura, Y. Mizukami, Y. Arai, Y. Sugimura, N. Maejima, A. Machida, T. Watanuki, T. Fukuda, T. Yajima, Z. Hiroi, K. Y. Yip, Y. C. Chan, Q. Niu, S. Hosoi, K. Ishida, K. Mukasa, S. Kasahara, J.-G. Cheng, S. K. Goh, Y. Matsuda *et al.*, Nat. Commun. **8**, 1143 (2017).

[27] J. Guo, S. Jin, G. Wang, S. Wang, K. Zhu, T. Zhou, M. He, and X. Chen, Phys. Rev. B **82**, 180520(R) (2010).

[28] Q.-Y. Wang, Z. Li, W.-H. Zhang, Z.-C. Zhang, J.-S. Zhang, W. Li, H. Ding, Y.-B. Ou, P. Deng, K. Chang, J. Wen, C.-L. Song, K. He, J.-F. Jia, S.-H. Ji, Y.-Y. Wang, L.-L. Wang, X. Chen, X.-C. Ma, and Q.-K. Xue, Chin. Phys. Lett. **29**, 037402 (2012).

[29] Y. Miyata, K. Nakayama, K. Sugawara, T. Sato, and T. Takahashi, Nat. Mater. **14**, 775 (2015).

[30] G. N. Phan, K. Nakayama, K. Sugawara, T. Sato, T. Urata, Y. Tanabe, K. Tanigaki, F. Nabeshima, Y. Imai, A. Maeda, and T. Takahashi, Phys. Rev. B **95**, 224507 (2017).

[31] M. Nakajima, K. Yanase, F. Nabeshima, Y. Imai, A. Maeda, and S. Tajima, Phys. Rev. B **95**, 184502 (2017).

[32] Y. Imai, Y. Sawada, F. Nabeshima, D. Asami, M. Kawai, and A. Maeda, Sci. Rep. **7**, 46653 (2017).

[33] F. Nabeshima, Y. Imai, M. Hanawa, I. Tsukada, and A. Maeda, Appl. Phys. Lett. **103**, 172602 (2013).

[34] Y. Sawada, F. Nabeshima, Y. Imai, and A. Maeda, J. Phys. Soc. Jpn. **85**, 073703 (2016).

[35] See Supplemental Material at http://link.aps.org/supplemental/10.1103/PhysRevResearch.3.L012007 for the evolution of the electronlike-FS shape and for the d_{xy}-band dispersion.

[36] S. V. Borisenko, D. V. Evtushinsky, Z.-H. Liu, I. Morozov, R. Kappenberger, S. Wurmehl, B. Büchner, A. N. Yaresko, T. K. Kim, M. Hoesch, T. Wolf, and N. D. Zhigadlo, Nat. Phys. **12**, 311 (2016).

[37] K. Kuroki, H. Usui, S. Onari, R. Arita, and H. Aoki, Phys. Rev. B **79**, 224511 (2009).

[38] Y. Yamakawa, S. Onari, and H. Kontani, Phys. Rev. X **6**, 021032 (2016).

[39] Y. Yamakawa and H. Kontani, Phys. Rev. B **96**, 144509 (2017).

[40] S. Lederer, Y. Schattner, E. Berg, and S. A. Kivelson, Phys. Rev. Lett. **114**, 097001 (2015).